Experimental Observation of Ultrashort Hyperchaotic Dark Multisoliton Complexes in a Magnonic Active Ring Resonator

Anastasia S. Bir, Sergei V. Grishin,* Olga I. Moskalenko, Alexey N. Pavlov, and Maksim O. Zhuravlev
Saratov State University, Saratov 410012, Russia

David Osuna Ruiz
College of Engineering, Department of Physics and Astronomy, University of Exeter, Exeter EX4 4QL, United Kingdom

(Received 12 October 2019; revised 6 June 2020; accepted 3 August 2020; published 21 August 2020)

We report on the self-generation of ultrashort hyperchaotic dark multisoliton sequences with two positive large Lyapunov exponents in an active ring resonator consisting of a multifunctional L-shaped magnonic waveguide and a saturable amplifier. The irregular magnonic waveguide supports the converting of backward volume magnetostatic spin waves with negative dispersion to magnetostatic surface spin waves with positive dispersion that is accompanied by a transition from four-wave to three-wave nonlinear spin-wave interactions. Each multisoliton complex consists of four dark parametric pulses containing the soliton trains of four dark incoherent spin-wave envelope solitons possessing a subnanosecond duration. Such patterns are formed due to the dispersion and nonlinearity management, the nonlinear transformation of the pulse signal in the saturable amplifier and the partial chaotic synchronization of both the ring eigenmodes and the spin wave automodulation frequencies. We also demonstrate a new intermittency type of "hyperchaotic multisoliton complexes-hyperchaotic multisoliton gas" with the increase of the signal power level.

DOI: 10.1103/PhysRevLett.125.083903

Dissipative solitons are the space- or time-localized patterns that are formed in the open and nonequilibrium systems due to a composite balance between dispersion or diffraction and nonlinearity as well as between gain and loss [1]. Among dissipative solitons, the multisoliton complexes (MSCs) occupy a special place. They are the bound states of several solitons that have been actively studied for the last two decades in nonlinear optics [1–3], Bose-Einstein condensates [4], and spin-wave electronics [5–10]. These patterns possess the inherent properties of a diatomic molecule of matter [2] and they are promising for applications such as stable upper bits in optical communications [3].

Nowadays, two mechanisms of the bound soliton formation are well known. One of them is based on the exploitation of a dispersive medium with two types of nonlinearities. The competition between quadratic and cubic nonlinearities provides the formation of spatial soliton clusters [11]. Another mechanism involves the usage of a nonlinear medium with the dispersion management when the temporal dispersion is periodically changed from positive to negative [2]. The periodic stretching and compression of pulses in a laser resonator based on a dispersion-managed optical fiber leads to the formation of the temporal dissipative MSCs consisting of the ultrashort pulses [12]. However, in nonlinear optics, the dispersion management is not accompanied by a periodic change in nonlinearity.

It is well known that solitons are asymptotically stable states of a dynamical system, while dynamical chaos is a result of the development of Lyapunov instability. In recent years, the unstable soliton states called *chaotic solitons* have been discovered [13–16]. The chaotic dynamics are diagnosed by the spectrum of Lyapunov exponents (LEs) characterizing the rate of recession of the phase trajectories [17]. For the dynamical chaos mode, the spectrum of LEs contains only one positive LE, whereas the presence of two or more positive LEs in the spectrum indicates the hyperchaos mode [18]. Hyperchaos was discovered in both finite-dimensional systems [19] and spatially distributed systems with an infinite number of degrees of freedom [20]. However, to our knowledge, no work has been devoted to the study of hyperchaos by means of LEs in distributed generators of MSCs.

Two years ago, a new pattern formation, the *chaotic dissipative MSCs*, were observed in a microwave active ring resonator based on two nonlinear elements: a regular magnonic waveguide and a fast saturable absorber based on a traveling wave tube suppressor [10]. The magnonic waveguide supported the propagation of a magnetostatic surface spin wave (MSSW) with positive waveguide dispersion that took part, simultaneously, in both three- and four-wave nonlinear spin-wave interactions. It led to the competition between quadratic and cubic nonlinearities. The microwave magnetic envelope (MME) solitons were formed through the modulation instability produced by the

nonlinearity competition. The bright parametric pulses contained either the quasiperiodic sequences of several bright MME solitons (a MSC) or the chaotic sequences of bound states of bright and dark MME solitons (a multisoliton gas). These structures were formed through the partial chaotic synchronization of either the ring eigenmodes or the spin wave (SW) automodulation frequencies. In both cases, the MME solitons had a duration of about several tens of nanoseconds, which was comparable to the duration of a single MME soliton circulating in the ring without the saturable absorber [9].

In the Letter, we demonstrate a self-generation of hyperchaotic MSCs consisting of both the dark parametric pulses and the dark envelope solitons of subnanosecond duration. To obtain such structures, we suggest using an L-shaped magnonic waveguide and an ultrawideband amplifier with a saturable output power in a feedback loop, as a ring resonator. The irregular magnonic waveguide implements the simultaneous management of dispersion and nonlinearity. The nonlinear amplifier is used for limiting the amplitude of the self-generated parametric pulses and expanding the power spectrum of the MSCs.

The experimental layout of the active ring resonator is shown in Fig. 1. Its main elements are the tangentially magnetized L-shaped magnonic waveguide, a cascade of two semiconductor amplifiers operating in the frequency band 2–4 GHz, and a variable attenuator. An input amplifier operates in a linear amplification mode and an output amplifier operates in a saturation mode of an output power. The signal power at the magnonic waveguide entrance is controlled by the variable attenuator. A two-channel power meter is used to measure the signal power at the entrances of both nonlinear elements. Most of the signal power returns to the ring from the output amplifier, and a small fraction goes to the input ports of a spectrum analyzer and a real-time oscilloscope.

The L-shaped magnonic waveguide is fabricated from a 13-μm-thick YIG film with a saturation magnetization of

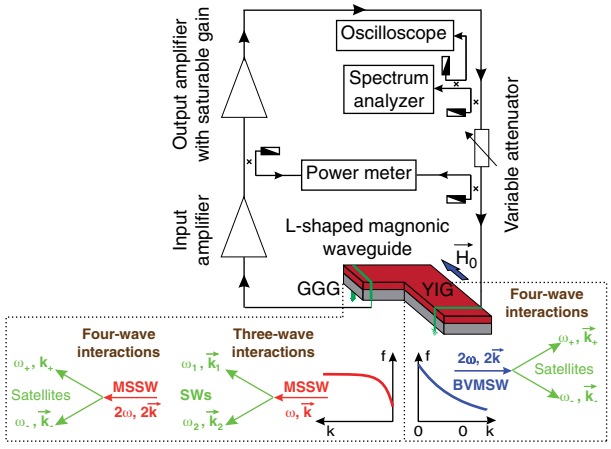

FIG. 1. Schematic diagram of a MSC oscillator.

$4\pi M_0 = 1750$ G grown on a 500-μm-thick gadolinium gallium garnet (GGG) substrate by the use of a liquid phase epitaxy technique. It has two segments (an "input arm" and an "output arm") placed in the external static magnetic field $H_0 = 627$ Oe. Both segments have a width of 950 μm and a length of $l = 4$ mm. The angle between them is 90°. Microstripe transducers with a width of 30 μm and a length of 1 mm are used for excitation and detection of the MSWs propagating in the magnonic waveguide. The magnetic field of H_0 is applied in the waveguide plane and directed longitudinally (perpendicularly) to the input (output) waveguide arms. Such magnetic field configurations support the propagation of both the backward volume MSWs (BVMSWs) with negative waveguide dispersion in the input arm and the MSSWs with positive waveguide dispersion in the output arm. The strength of H_0 is chosen in such a way that only four-wave nonlinear interactions are allowed for the BVMSWs, and three- and four-wave nonlinear interactions can coexist for the MSSWs.

A distinctive feature of the irregular L- and T-shaped magnonic waveguides, in contrast to regular magnonic waveguides, is the ability to convert the MSW waveguide dispersion [21,22], that may be accompanied by the transition from one type of nonlinear interaction to another. The different orientation of the irregular waveguide segments relative to the direction of the field H_0 is the main cause of both conversions. These conversions are effective for the waveguide width ≤ 1 mm because each waveguide segment has different internal magnetic fields H_{int}.

Figure 2(a) shows the dispersion characteristics of the BVMSW and MSSW lowest thickness modes calculated based on well-known dispersion equations [23]. The calculations are performed for two values of H_{int} (H_{int1} and H_{int2}) corresponding to the internal magnetic field values of both segments of the L-shaped waveguide. It is shown that there is a frequency region (highlighted in color) in which the dispersion conversion is possible due to the intersection of the dispersion curves of the BVMSW and MSSW. If we take into account the width modes of both MSWs, then the frequency range of the dispersion conversion will be much wider [22]. Following the results presented in Fig. 2(c), the conversion of the BVMSW width modes into the MSSW width modes leads to the formation of the amplitude-frequency response (AFR) of the "comb" type [21]. Inside the largest peak of the comb, the time of the MSW propagating through the L-shaped waveguide τ_{MSW} is initially increased and is decreased with increasing frequency [see the inset in Fig. 2(c)] [21]. As shown in Fig. 2(b), such behavior of the $\tau_{\text{MSW}}(f)$ leads to a change in the average group velocity dispersion (GVD) $D_{\text{av}}^{\text{irreg}} = dV_{g,\text{av}}/dk$ (where $V_{g,\text{av}} = l/\tau_{\text{MSW}}$, k is a MSW wave number) from negative to positive. The zero value of the GVD corresponds to the largest peak frequency $f_0 = 3384$ MHz of the AFR at which a monochromatic microwave signal will be self-generated in the active ring

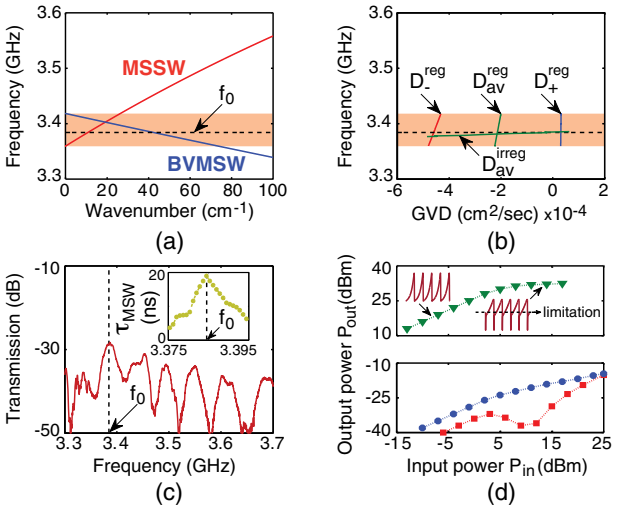

FIG. 2. The dispersion characteristics (a) and the frequency dependencies of group velocity dispersion (b) of MSWs for two magnetic field configurations. For the BVMSW field configuration, the internal magnetic field is $H_{\text{int1}} = H_0$ and for the MSSW filed configuration,—$H_{\text{int2}} = H_0 + H_d$, where $H_d = -17$ Oe is a demagnetizing field. In (c), there are the amplitude-frequency and MSW time propagation-frequency responses of the L-shaped waveguide. In (d), there are the $P_{\text{out}}(P_{\text{in}})$ responses of the output amplifier (top panel) and the L-shaped waveguide (bottom panel) measured at the frequencies f_0 (triangles and circles) and f_1 (squares).

resonator. By analogy with optics, we can talk about the dispersion management of the MSW in the L-shaped magnonic waveguide. Figure 2(b) shows also the frequency dependencies of the BVMSW and MSSW GVD (D_{+}^{reg} and D_{-}^{reg}), as well as the average GVD $D_{av}^{\text{reg}} = (D_{+}^{\text{reg}} + D_{-}^{\text{reg}})/2$ calculated for the wide regular magnonic waveguides. The obtained results demonstrate that the MSW dispersion management can not be implemented here, because $D_{\text{av}}^{\text{reg}} \sim D_{-}^{\text{reg}}$.

Besides the dispersion management, the irregular magnonic waveguides also support three- and four-wave nonlinear spin-wave interactions, whose characteristic times are very different from each other and depend on the MSW amplitude. It is well known [24], that four-wave interactions have no frequency limitation and exist in all frequency range of the MSW excitation. On the contrary, three-wave interactions are limited by the upper frequency thresholds that have the values of $f_{\text{th1}} \cong 3.3$ GHz ($H_{\text{th1}} = 583$ Oe) for the BVMSW and $f_{\text{th2}} \cong 4.9$ GHz ($H_{\text{th2}} = 875$ Oe) for the MSSW field configurations. In our case, three-wave interactions exist only for the MSSW field configuration, because $H_{\text{int2}} < H_{\text{th2}}$ and $H_{\text{int1}} > H_{\text{th1}}$. The power thresholds for three-wave interactions are at least an order of magnitude less than for four-wave interactions. However, if the MSW amplitude is sufficiently large, then both nonlinear processes can develop simultaneously, which leads to the competition between the nonlinearities [10].

In the L-shaped magnonic waveguide, we can realize the nonlinearity management, where one waveguide arm supports four-wave interactions and the other arm supports three-wave interactions. It is realized in some frequency range $f_{\text{th}} \le f \le f_{\text{th2}}$ (where $f_{\text{th}} = 2f_H = 3416$ MHz, $f_H = \gamma H_{\text{int2}}$ is a frequency of the "spin wave bottom," below which parametrically excited SWs do not exist, and γ is a gyromagnetic ratio), in which a frequency $f_1 = 3464$ MHz (a carrier frequency of a multifrequency pulse signal generated in the ring) is placed. For the frequency f_0, the nonlinearity management is absent, because $f_0 < f_{\text{th}}$.

In Fig. 2(d) (bottom panel), there are the responses of the output power versus input power of the L-shaped waveguide that are measured at f_0 and f_1. It is shown that at f_1, the nonlinearity management leads to the growth of MSW nonlinear loss that is much greater than MSW nonlinear loss at f_0. In Fig. 2(d) (top panel), we also demonstrate the output amplifier power response saturation at the input power of $P_{\text{in}} = +5$ dBm. Thus, the output amplifier is a power limiter that effectively amplifies the small amplitude signals and limits the large amplitude signals. If the parametric relaxation pulses of a high peak power level are fed into the amplifier entrance, then the amplifier will limit their amplitude, as shown in an inset of Fig. 2(d). As a result, a plateau of constant amplitude will be formed from each parametric pulse of a sequence and separated from the neighboring plateau by a narrow dip, similar to a "dark" pulse. The duration of the dip will be decreased due to the broadening of the pulse signal spectrum by the output nonlinear amplifier.

In Fig. 3, there are the spectral and temporal responses of a dark multisoliton sequence self-generated in the active ring resonator at a ring gain of $G = 9.85$ dB (where $G = K - A$, K is a gain of the amplifier cascade and A is the total loss in the ring). At the entrance of the L-shaped waveguide, an average power of the self-generated pulse signal is $P_{\text{av}} = +18$ dBm and at the entrance of the output amplifier is $P_{\text{av}} \simeq +10$ dBm. At these power levels, the nonlinearity management is realized in the irregular waveguide and the nonlinear amplifier operates in the output power saturation mode [see Fig. 2(d)]. The power spectrum of the generated pulse signal [see Fig. 3(a)] is broadband (more than 1 GHz) and contains a frequency comb with a carrier frequency of f_1.

In the time domain [see Fig. 3(b)], a sequence of wide dips containing a fine structure of the dips of shorter duration is observed. The wide dips are the dark parametric pulses, that are formed due to the limitation of the parametric relaxation pulse amplitude by the output nonlinear amplifier. Four dark parametric pulses form a temporary pattern, an enlarged fragment of which is shown in Fig. 3(d)ii. The temporal pattern has a repetition frequency of $f_{\text{am}} \cong 500$ kHz, corresponding to the automodulation frequency of SWs. The frequency separation between the parametric pulses within the pattern varies from 1.8 to

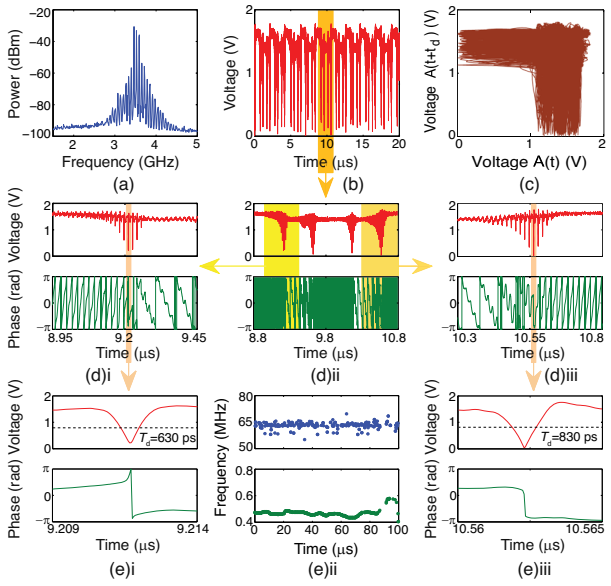

FIG. 3. (a) Microwave power-frequency spectrum, (b) envelope amplitude profile, and (c) envelope phase map of the hyperchaotic dark multisoliton train. In (d),(e), there are enlarged fragments of envelope amplitude (top panel) and phase (bottom panel) profiles of (d)ii a MSC consisting of four dark parametric pulses; (d)i and (d)iii single dark parametric pulses containing the trains of four dark envelope solitons; (e)i and (e)iii single subnanosecond dark envelope solitons possessing the greatest amplitude dip. In (e)ii, there is a frequency-time map for two specific frequencies of the MSCs.

2.5 MHz. These values correspond to the values of satellite frequencies that arise as a result of three-wave confluence processes [25].

In Figs. 3(d)i,iii, there are the enlarged fragments of two dark parametric pulses that are inside the same temporal pattern. It is shown, that each dark parametric pulse contains about ten narrower dips similar to the dark MME solitons. The time interval between neighboring solitons of the fine structure depends on the frequency separation between the ring eigenmodes, which determines the repetition rate of solitons $f_r \cong 65$ MHz. A detailed study of the amplitude and phase profiles of the dark envelope solitons showed that a relative phase between the neighboring solitons is different from 2π and approximately equal to $\pi/2$. As follows from theoretical predictions [26], such a phase difference between solitons is necessary for the stable dissipative soliton bound state formation. In our case, the stable bound state of four dark envelope solitons simultaneously circulates in the ring and forms the soliton trains inside each dark parametric pulse. The central soliton of the train can be either black or gray soliton. In Fig. 3(e)iii, the amplitude inside the central soliton goes to zero and the phase has a jump equal to π that corresponds to a black envelope soliton [9]. In Fig. 3(e)i, such conditions are not strictly fulfilled and this is the case of a gray envelope soliton [9]. At the same time, both (black and gray) envelope solitons have ultrashort durations (< 1 ns), that was not previously observed for the fundamental MME solitons [9].

In our opinion, the self-generation of the dark envelope solitons of subnanosecond duration is connected with the simultaneous use of the L-shaped magnonic waveguide and the nonlinear ultrawideband amplifier in the ring. In the Supplemental Material [27], we demonstrate the formation of wider dark envelope solitons with the same amplifier, but now with a regular magnonic waveguide that supports only the MSSW propagation. In this generator scheme, the nonlinearity management is absent and, instead, the competition between three- and four-wave nonlinear interactions at the dominant eigenmode frequency is present. As a result, there are no MSCs containing the dark envelope soliton trains of ultrashort duration, and only single modulated dark envelope solitons are observed. Their duration is 4 times longer than the duration of the ultrashort solitons.

In contrast to the single soliton formations, the dark MSCs are formed through the partial synchronization of both ring eigenmodes and the SW automodulation frequencies. A frequency-time map presented in Fig. 3(e)ii demonstrates that two specific frequencies f_r (top panel) and f_{am} (bottom panel) slightly vary over time near their constant values, thus providing a partial synchronization of both the ring eigenmodes and the SW automodulation frequencies. The complex structure of the phase map [see Fig. 3(c)] indicates that the self-generated pulses can have a chaotic nature. To confirm it, two large LEs were calculated from the experimental time series. The calculations were carried out according to the algorithm described in Ref. [28]. It was established that both LEs are positive and have the values of $\lambda_1 = 8.19$ and $\lambda_2 = 6.93$ $\mu\mathrm{s}^{-1}$ that are averaged over the length of the time series. Their positive values indicate that the multisoliton sequence is hyperchaotic.

In Fig. 4, the transition from the MSCs to the multisoliton gas through a new intermittency type is demonstrated. So, at $G = 10.6$ dB [see Fig. 4(a)] the sequence of the hyperchaotic dark MSCs with $\lambda_1 = 12.6$ and $\lambda_2 = 9.45$ $\mu\mathrm{s}^{-1}$ is still self-generated. The increase of the ring gain to $G = 11.6$ dB [see Figs. 4(b)iii] leads to the desynchronization of the frequencies f_r and f_{am} at some time intervals. As a result [see Figs. 4(b)i,ii], the hyperchaotic dark MSCs alternate with the hyperchaotic dark multisoliton gas possessing different local LEs ($\lambda_{l1} = 14.49$, $\lambda_{l2} = 6.3$ $\mu\mathrm{s}^{-1}$ for MSCs [see Fig. 4(b)ii, top panel] and $\lambda_{l1} = 57.96$, $\lambda_{l2} = 39.69$ $\mu\mathrm{s}^{-1}$ for multisoliton gas [see Fig. 4(b)ii, bottom panel]). At $G = 12.6$ dB, the partial chaotic synchronization of the frequencies f_r and f_{am} is violated in all time intervals [see Fig. 4(c)iii] and only hyperchaotic dark multisoliton gas [see Fig. 4(c)i] with $\lambda_1 = 69.3$ and $\lambda_2 = 47.88$ $\mu\mathrm{s}^{-1}$ [see Fig. 4(c)ii] is self-generated.

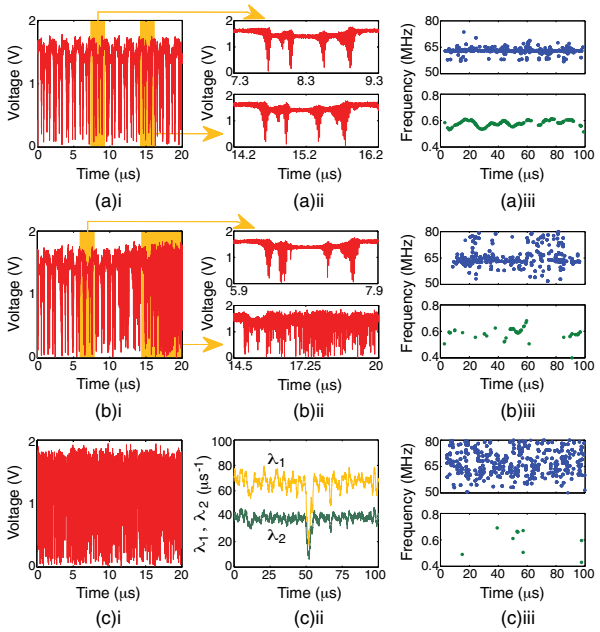

FIG. 4. (a)i,(b)i,(c)i: Envelope amplitude profiles, (a)ii,(b)ii: their enlarged fragments, (a)iii,(b)iii,(c)iii: frequency-time maps for two specific frequencies f_r (top panel) and f_{am} (bottom panel) as well as (c)ii temporal dependencies of two large LEs of multisoliton sequences obtained for several values of G: (a) 10.6, (b) 11.6, and (c) 12.6 dB.

In conclusion, we note that the dispersion and nonlinearity management in conjunction with the limiting function of the amplifier may be used in other dissipative systems with gain to form the dark MSCs of ultrashort duration. The obtained results may be of interest both to researchers in the field of nonlinear dynamics, and to specialists involved in the creation of ultrashort pulse sources for microwave and optical communications.

The mathematical processing of time series and the estimation of the large Lyapunov exponents were supported by the Russian Foundation for Basic Research (Project No. 19-02-00075). The development of a generator layout and experimental studies of the multisoliton complex modes were supported by the Russian Scientific Foundation (Project No. 16-19-10283).

*sergrsh@yandex.ru

[1] N. Akhmediev and A. Ankiewicz, *Dissipative Solitons: From Optics to Biology and Medicine* (Springer-Verlag, Berlin, 2008).
[2] M. Stratmann, T. Pagel, and F. Mitschke, Phys. Rev. Lett. **95**, 143902 (2005).
[3] P. Grelu and N. Akhmediev, Nat. Photonics **6**, 84 (2012).
[4] K. Lakomy, R. Nath, and L. Santos, Phys. Rev. A **86**, 013610 (2012).
[5] B. A. Kalinikos, N. G. Kovshikov, and C. E. Patton, JETP Lett. **68**, 243 (1998).
[6] B. A. Kalinikos, N. G. Kovshikov, M. P. Kostylev, and H. Benner, JETP Lett. **76**, 253 (2002).
[7] S. O. Demokritov, A. A. Serga, V. E. Demidov, B. Hillebrands, M. P. Kostylev, and B. A. Kalinikos, Nature (London) **426**, 159 (2003).
[8] A. B. Ustinov, B. A. Kalinikos, V. E. Demidov, and S. O. Demokritov, Phys. Rev. B **80**, 052405 (2009).
[9] M. Wu, Solid State Phys. **62**, 163 (2010).
[10] S. V. Grishin, B. S. Dmitriev, O. I. Moskalenko, V. N. Skorokhodov, and Y. P. Sharaevskii, Phys. Rev. E **98**, 022209 (2018).
[11] Y. V. Kartashov, L. C. Crasovan, D. Mihalache, and L. Torner, Phys. Rev. Lett. **89**, 273902 (2002).
[12] K. Krupa, K. Nithyanandan, U. Andral, P. Tchofo-Dinda, and P. Grelu, Phys. Rev. Lett. **118**, 243901 (2017).
[13] S. R. Bolton and M. R. Acton, Phys. Rev. A **62**, 063803 (2000).
[14] N. Akhmediev, J. M. Soto-Crespo, and G. Town, Phys. Rev. E **63**, 056602 (2001).
[15] E. N. Beginin, S. V. Grishin, and Y. P. Sharaevsky, JETP Lett. **88**, 647 (2008).
[16] Z. Wang, A. Hagerstrom, J. Q. Anderson, W. Tong, M. Wu, L. D. Carr, R. Eykholt, and B. A. Kalinikos, Phys. Rev. Lett. **107**, 114102 (2011).
[17] A. Liapounoff, Ann. Fac. Sci. Univ. Toulouse **9**, 203 (1907).
[18] S. P. Kuznetsov and D. I. Trubetskov, Radiophys. Quantum Electron. **47**, 341 (2004).
[19] T. Meyer, M. J. Bunner, A. Kittel, and J. Parisi, Phys. Rev. E **56**, 5069 (1997).
[20] A. E. Hramov, A. A. Koronovskii, V. A. Maximenko, and O. I. Moskalenko, Phys. Plasmas **19**, 082302 (2012).
[21] A. V. Sadovnikov, C. S. Davies, V. V. Kruglyak, D. V. Romanenko, S. V. Grishin, E. N. Beginin, Y. P. Sharaevskii, and S. A. Nikitov, Phys. Rev. B **96**, 060401(R) (2017).
[22] A. V. Sadovnikov, C. S. Davies, S. V. Grishin, V. V. Kruglyak, D. V. Romanenko, Yu. P. Sharaevskii, and S. A. Nikitov, Appl. Phys. Lett. **106**, 192406 (2015).
[23] B. A. Kalinikos and A. N. Slavin, J. Phys. C **19**, 7013 (1986).
[24] V. S. L'vov, *Wave Turbulence Under Parametric Excitation* (Springer-Verlag, Berlin, 1994).
[25] S. V. Grishin and Y. P. Sharaevskii, JETP Lett. **89**, 53 (2009).
[26] N. N. Akhmediev, A. Ankiewicz, and J. M. Soto-Crespo, Phys. Rev. Lett. **79**, 4047 (1997).
[27] See Supplemental Material at http://link.aps.org/supplemental/10.1103/PhysRevLett.125.083903 for demonstration of the wider dark envelope soliton self-generation in the active ring resonator with a regular magnonic waveguide.
[28] A. Wolf, J. B. Swift, H. L. Swinney, and J. A. Vastano, Physica (Amsterdam) **16D**, 285 (1985).